DETERMINATION AND TESTING OF PELLETIZED COATED PARTICLES
/
丸化包衣颗粒的测定与试验

Min LIU, Zhanfeng HOU*, Xuejie MA, Xiwen ZHANG, Nianzu DAI
Inner Mongolia Agricultural University, College of Mechanical and Electrical Engineering, Inner Mongolia, China
*Tel: +86 04714309215; *)Corresponding author E-mail: njauhzf@163.com*
DOI: https://doi.org/10.35633/inmateh-66-25

Keywords: *Coated powder; Alfalfa seeds; Resting angle; Discrete elements; Parameter calibration*

ABSTRACT
The calibration of the powder simulation parameters could improve the accuracy of the pelletizing and coating simulation process. In this paper, we take coated powder (after this referred to as powder) as the research object, based on particle amplification theory, combined with physical tests to calibrate the contact parameters of powder and seeds (after this referred to as seeds), conduct the angle of repose simulation tests of powder, carry out Plackett-Burman test, steepest climb test, and Box-Behnken test in turn, and establish quadratic regression equation to obtain the best combination of powder simulation parameters. The difference between the contact parameter combinations obtained from the simulation tests and the physical test results is less than 1%, providing some reference for calibrating similar powder material parameters.

摘要
为对粉料仿真参数进行标定，可提高丸化包衣仿真过程的准确性。本文以包衣粉料（以下简称粉料）作为研究对象，基于颗粒放大理论，结合物理试验标定紫花苜蓿种子（以下简称种子）与粉料间的接触参数；进行粉料休止角仿真试验，依次开展Plackett-Burman试验、最陡爬坡试验与Box-Behnken试验，建立二次回归方程，得到粉料最佳仿真参数组合。仿真试验得到接触参数组合与物理试验结果相差均小于1%，为相似粉体物料参数标定提供一定参考。

INTRODUCTION

Seed pellet coating technology is a processing technology in which seeds, seed coating agents, coating powders, and additives with other active ingredients are mixed in a specific ratio, wrapped evenly and effectively on the surface of the seeds using seed coating equipment as a carrier to protect the seeds from external biotic or abiotic attack and thus improve the seed viability and germination rate (*Zhao, 2009; Afzal, 2020*). By using the discrete element method to analyse the seed pellet coating process, the forces of the particles, of the particles and the working parts can be taken into account, which improves the accuracy of the application of the discrete element method when analysing the seed pellet coating process (*Zeng, 2021*). The powder is a typical bulk material with complex physical properties (*Jaeger, 1997; Liu, 2017*). Considering that the powder is prone to bonding during the test, we chose the JKR (Johnson-Kendall-Roberts) model as the contact model. The JKR model introduces the concept of particle surface energy, which is more suitable for studying small particle powder materials, crops, soil, and other wet materials and could simulate the bonding agglomeration between particles (*Luo, 2018; Johnsonkl, 1971*).

Domestic and foreign scholars have conducted much research on agricultural materials based on the discrete element method. *Boac*, *(2009),* summarized the crop material and contact parameters to verify the accuracy of the simulation test using soybean as an example and obtained the best combination of parameters for the simulation test on soybean. *John*, *(2019),* scaled up the cellulose using a coarse-grained approach and calibrated the model using a genetic algorithm. *LaTosha, (2013),* determined the collision recovery coefficient of coal particles and found that the bounce angle has a significant effect on the collision recovery coefficient of particles. *Zeebroeck*, *(2006),* applied the discrete element method to apple abrasion experiments for the first time, using a single sphere model in EDM to simulate apples, and selected the Kuwabara-and-Kon contact model to carry out simulation tests. *Ma, (2020),* conducted resting angle tests on compressed alfalfa straw powder and established a second-order regression model to obtain the best combination of simulation parameters for alfalfa straw. *Thomas, (2016),* analyses the effect of coarse grain size on the accuracy of simulation tests within a silo flow model based on EDEM.

Mukherjee, (2018), proposes a discrete element model to predict the effect of humidity on drug powder flow by varying the cohesion between particles in a simple hopper geometry. *ASAF, (2007),* established a two-dimensional model of soil particles and sought the optimal soil contact parameters by the Nelder-Mead algorithm. *Alexandros*, *(2020)*, simulated the mobility of the powder at low pressure by DEM and found that the coefficient of friction between the particles affects the confinement factor. *Mohammadreza, (2018),* used the discrete element method to analyse the effect of inter-particle adhesion force on simulation accuracy during powder mixing. *Xing, (2020),* used the JKR model to calibrate soil contact parameters using soil in the hot zone of Hainan. *Li, (2019),* based on particle scaling theory, uses the discrete element method to obtain the optimum combination of contact parameters for wheat flour. *Tamas, (2018),* developed a discrete element simulation model of the soil sweeper and calibrated the soil under different moisture content conditions. Comprehensive domestic and international research status: few studies on the calibration of powder material parameters, and no discrete element simulation parameter calibration for coated powder has been seen.

In this paper, we measure the basic physical parameters of powders by physical experiments combined with simulation tests, and the rest angle is used as the response value for simulation tests to establish the regression equation and obtain the optimal combination of simulation contact parameters for powders, in order to provide a reference for the calibration of discrete element parameters of other powder materials.

MATERIALS AND METHODS

Test material and parameter determination

The experiment uses the seeds and the powder which made up of soybean meal and diatomaceous earth as the radio of 1:1 as the material, and the seed simulation parameters were measured by physical tests (*Hao, 2017*), combining the domestic and international literature and referring to the built-in database of EDEM software (*Zhou, 2017*), the powder simulation parameters were obtained, as shown in Table 1.

Table 1

Discrete element simulation test parameters

Simulation parameters	Values
Poisson's ratio of seed	0.4
Seed shear modulus / Pa	1.02×10^{7}
Seed density / kg·m^{-3}	1250±0.016
Poisson's ratio of powder	0.296
Powder shear modulus / Pa	3×107
Powder density / kg·m^{-3}	1833±0.1

Simulation Model

The powder and seed simulation models were established in the discrete element simulation software, and the powder particles used a single spherical model, as shown in Figure 1a, and the particle size was enlarged by 6 times based on the particle amplification theory (*Feng, 2009; Thakur, 2016; Sakai, 2014*). The seeds used a multi-sphere aggregation to establish the discrete element simulation model, as shown in Figure 1b. We chose the Hertz-Mindlin no-slip contact model to conduct the contact parameter calibration test between seed and powder (*Wu, 2019*) and chose the Hertz-Mindlin with JKR contact model for conducting the powder rest angle simulation test. We used the fixed-size particles for the simulation, with a Rayleigh Time Step of 6.87 × 10-6s and a grid size of 3R_{min} (*Hu, 2010*).

a. Powder particle b. Alfalfa seed

Fig. 1 - Simulation model of alfalfa seeds and powder

PARAMETER CALIBRATION PROCESS

Powder to seed contact parameter calibration

Crash recovery factor

This paper used the collision bounce test to calibrate the collision recovery coefficient of seeds and powder, as shown in Figure 2.

Since the static friction coefficient a_2 and rolling friction coefficient a_3 between seed and powder, the collision recovery coefficient a_4, static friction coefficient a_5, and rolling friction coefficient a_6 between powders do not affect the seed rebound height, they are all set to 0. Take the range of collision recovery coefficient of seed and powder a_1 is 0.1~0.3, the step size is 0.05 for 6 sets of tests, and get the rebound height of seed b_1, the test design and results are shown in Table 3, and the fitting equation is shown in Eq. 1.

a. Physical tests b. Simulation test

Fig. 2 - Collision recovery coefficient test

Table 3

Collision recovery coefficient test design and results

No.	a_1	b_1 / mm
1	0.10	2.499
2	0.15	4.615
3	0.20	6.09
4	0.25	8.502
5	0.30	9.809
6	0.35	13.39

$$b_1 = 20.01479\,a_1 + 47.52143\,a_1^{\,2} + 0.22856 \quad (1)$$

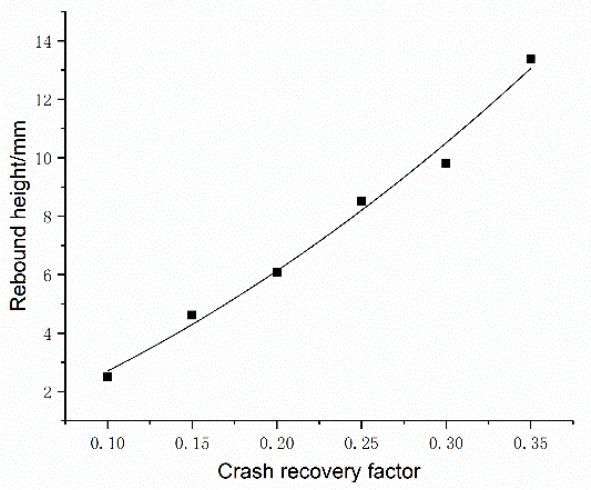

Fig. 3 - Collision recovery coefficient and rebound height fitting curve

The coefficient of determination of the fitted equation R^2=0.98904 indicates that the equation fits reliably, and the rebound height of 8.01 mm measured by the physical experiment is brought into the equation, and the solution of a_1 is 0.246. The solution result is input into EDEM for the simulation test, and the rebound height is 8.07, and the relative error is only 0.75%.

Static friction coefficient

In this paper, we use the slope method to determine the static friction coefficient of seed and powder, and the test is shown in Figure 4. When conducting the slope slip simulation test, set a_1 as 0.246, set a_3, a_4, a_5, and a_6 to 0. Take the range of static friction coefficient between seed and powder a_2 from 0.6 to 0.85, set the step size to 0.02 for 6 sets of tests and obtain the rotation angle b_2 of the inclinometer. The test design and results are shown in Table 4, and the fitting equation is shown in Eq.2.

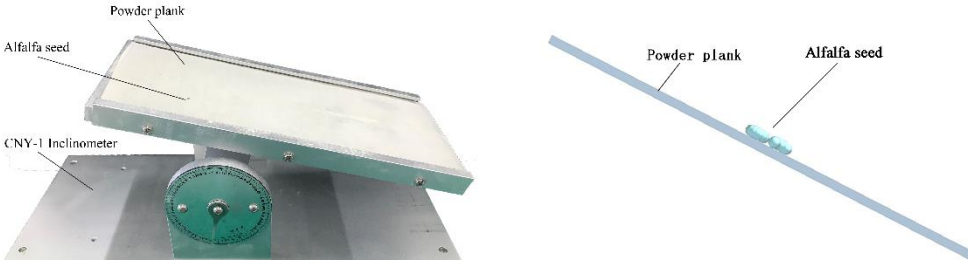

a. Physical tests b. Simulation test

Fig. 4 - Slope slip test

Table 4

Design and results of slope sliding test

No.	a_2	b_2 / mm
1	0.7	20.4
2	0.72	22.86
3	0.74	24.12
4	0.76	29.04
5	0.78	32.76
6	0.8	37.8

$$b_2 = -1349.025a_2 + 1015.17857a_2^2 + 467.37643 \quad (2)$$

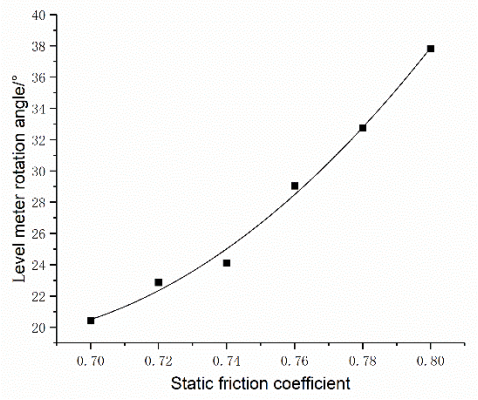

Fig. 5 - Fitting curve of static friction coefficient and rotation angle of inclinometer

The coefficient of determination of the fitted equation R^2=0.98904, the physical test result of 31.85° was brought into the equation, and the solution of a_2 was 0.776. The solution result was input into EDEM for the simulation test, and the rotation angle was 32.06°, and the relative error with the physical test was 0.66%.

Rolling friction coefficient

This paper determined the rolling friction coefficient between seeds and powders by an inclined rolling test, shown in Figure 6. When conducting the inclined rolling simulation test, set a_1 as 0.246, set a_2 as 0.776, set a_4, a_5, and a_6 to 0. The rolling friction coefficient of seed and powder a_3 was taken to be in the range of 0.2-0.3, set a step size of 0.02 for six sets of simulation tests. b_3 was the horizontal rolling distance of seeds, and the experimental design and results are shown in Table 5, and the fitting equation is shown in Eq.3.

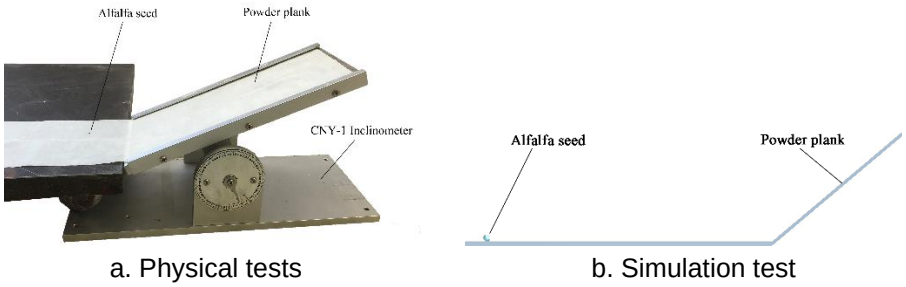

a. Physical tests b. Simulation test

Fig. 6 - Inclined rolling test

Table 5

Inclined rolling test design and results

No.	a_3	b_3 / mm
1	0.2	114.6
2	0.22	93.12
3	0.24	81.51
4	0.26	63.08
5	0.28	56.00
6	0.3	39.88

$$b_3 = -1721.80714\,a_3 + 2005.35714\,a_3^2 + 377.47571 \quad (3)$$

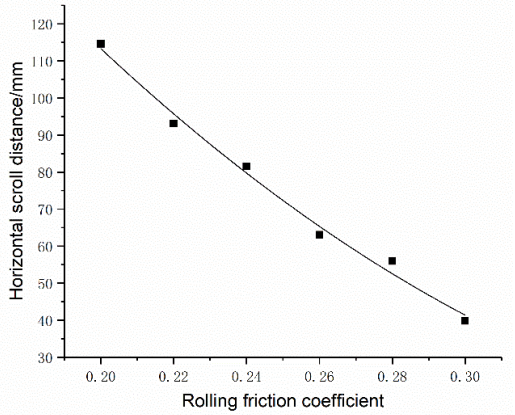

Fig. 7 - Fitting curve of rolling friction coefficient and horizontal rolling distance

The coefficient of determination of the fitted equation R^2=0.99102, the physical test result of 69.2mm was brought into the equation and solved to obtain a_3 of 0.255. The solution result was input into EDEM for the simulation test, and the seed horizontal rolling length was 68.74mm, with a relative error of 0.66% from the physical test.

Contact parameter calibration test of the powder

The angle of the repose test

Using FT-104B resting angle tester for powder resting angle test, as in Figure 8a, the profile curve is extracted by image processing and linearly fitted to obtain the simulation test rest angle, as shown in Figure 9, the average value was obtained as 41.69°±0.79.

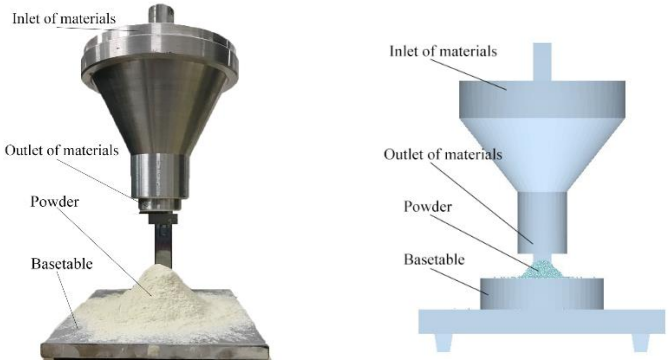

a. FT-104B resting angle tester b. Resting angle simulation model

Fig. 8 - Angle of Repose Test

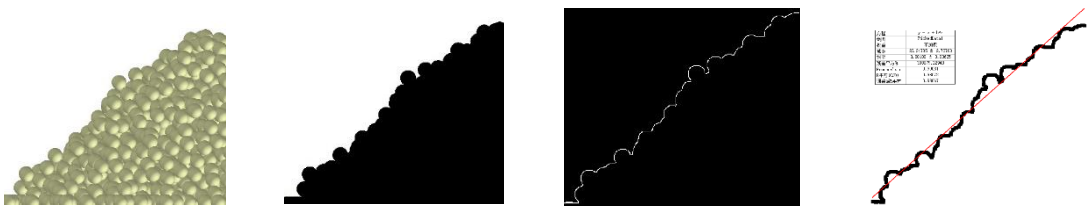

a. Original image b. Binarization c. Boundary extraction d. Linear fitting

Fig. 9 - Image processing

The Plackett-Burman test

The Plackett-Burman test was conducted with the rest angle as the response value, and the test parameters are shown in Table 6, and the test design and results are shown in Table 7.

Table 6

Plackett-Burman test parameters range table

Simulation test parameters	Low level (-1)	High level (+1)
Powder - powder restitution coefficient *A*	0.05	0.25
Powder - powder static friction coefficient *B*	0.7	0.9
Powder - powder rolling friction coefficient *C*	0.25	0.45
Powder - steel plate restitution coefficient *D*	0.05	0.25
Powder - steel plate static friction coefficient *E*	0.62	0.82
Powder - steel plate rolling friction coefficient *F*	0.19	0.39
JKR surface energy *G*	0.1	0.3

Table 7

Plackett-Burman test protocol and results No.	*A*	*B*	*C*	*D*	*E*	*F*	*G*	Repose angle θ / °
1	1	1	-1	1	1	1	-1	30.86
2	-1	1	1	-1	1	1	1	48.00
3	1	-1	1	1	-1	1	1	49.16
4	-1	1	-1	1	1	-1	1	39.11
5	-1	-1	1	-1	1	1	-1	42.73
6	-1	-1	-1	1	-1	1	1	41.45
7	1	-1	-1	-1	1	-1	1	44.82
8	1	1	-1	-1	-1	1	-1	33.91
9	1	1	1	-1	-1	-1	1	44.41
10	-1	1	1	1	-1	-1	-1	38.53
11	1	-1	1	1	1	-1	-1	43.24
12	-1	-1	-1	-1	-1	-1	-1	32.78
13	0	0	0	0	0	0	0	43.74

Table 8

Plackett-Burman test parameter contribution analysis

Parameters	Stdized effects	Sum of squares	Contribution degree / %
A	0.63	1.20	0.31
B	-3.23	31.23	8.05
C	7.19	155.09	39.99
D	-0.72	1.54	0.40
E	1.42	6.05	1.56
F	0.54	0.86	0.22
G	7.48	168.00	43.32

Table9

Significance analysis of Plackett-Burman test parameters

Parameters	Degree of freedom	Sum of squares	F-value	P-value
Model	7	363.98	13.32	0.0124
A	1	1.20	0.31	0.6084
B	1	31.23	8.00	0.0474*
C	1	155.09	39.72	0.0032**
D	1	1.54	0.39	0.5640
E	1	6.05	1.55	0.2812
F	1	0.86	0.22	0.6626
G	1	168.00	43.03	0.0028**

*Note: ** indicates an extremely significant effect (p<0.01),* indicates a significant effect (p<0.05). Same as below*

From Table 8 we can obtain the effect of each parameter on the rest angle and the contribution rate, where *A*, *C*, *E*, *F*, and *G* have a positive effect on the powder rest angle, the rest angle will increase with the increase of this parameter, and *B* and *D* harm the powder rest angle, the rest angle will decrease with the increase of this parameter (*Peng, 2020*). The contribution of each parameter to the resting angle of the powder is analysed, and the top 3 contributing parameters are *G*, *C*, and *B*, and combined with the significance analysis of the test parameters in Table 9, it was obtained that *G* has a highly significant effect on the resting angle, C and *B* have a significant effect on the resting angle.

The Steepest climb test

Design the steepest climb test according to the parameter effect on the three screened significant parameters; the test design and results are shown in Table 10.

Table 10

Steepest climb test design scheme and results

No.	Powder-powder static friction coefficient, *B*	Powder-powder rolling friction coefficient, *C*	JKR surface energy, / J·m^{-2}, *G*	Relative error / %
1	0.9	0.25	0.1	22.91
2	0.86	0.29	0.14	0.50
3	0.82	0.33	0.18	2.64
4	0.78	0.37	0.22	4.41
5	0.74	0.41	0.26	6.86
6	0.7	0.45	0.30	31.66

The Box-Behnken test

Based on the steepest climb test results, the screened significant parameters were ranked as low, medium, and high levels then the Box-Behnken test was conducted. The test parameter levels are shown in Table 11; the test design scheme and results are shown in Table 12.

Table 11

Parameter level coding table

Levels	Powder-powder static friction coefficient *B*	Powder-powder rolling friction coefficient *C*	JKR surface energy / J·m^{-2}, *G*
-1	0.9	0.25	0.1
0	0.86	0.29	0.14
+1	0.82	0.33	0.18

Table 12

Box-Behnken test protocol and results

No.	Powder-powder static friction coefficient *B*	Powder-powder rolling friction coefficient *C*	JKR surface energy *G*	Repose angle *θ* / °
1	-1	-1	0	36.41
2	1	-1	0	36.96
3	-1	1	0	42.25
4	1	1	0	42.33
5	-1	0	-1	32.76
6	1	0	-1	37.86
7	-1	0	1	38.91
8	1	0	1	38.43
9	0	-1	-1	30.62
10	0	1	-1	38.69
11	0	-1	1	37.21
12	0	1	1	39.96
13	0	0	0	40.55
14	0	0	0	41.17
15	0	0	0	41.53
16	0	0	0	41.31
17	0	0	0	41.7

Table 13

Box-Behnken test regression model analysis of variance

Source	Mean square	Degree of freedom	Sum of square	P-value
Model	18.85	9	169.61	<0.0001**
B	3.45	1	3.45	0.0244*
C	60.67	1	60.67	<0.0001**
G	26.57	1	26.57	<0.0001**
BC	0.0552	1	0.0552	0.7281
BG	7.78	1	7.78	0.0036**
CG	7.08	1	7.08	0.0046**
B^2	2.05	1	2.05	0.0634
C^2	4.80	1	4.80	0.0119*
G^2	53.51	1	53.51	<0.0001**
Residual	0.4218	7	2.95	
Lack of fit	0.7238	3	2.17	0.1190
Pure error	0.1952	4	0.7809	
Sum		16	172.56	

Using Design-Expert 11.0 software to perform multiple regression analysis on the experimental data, the second-order regression equation for the relative error of the rest angle was obtained as follows:

$$\begin{aligned} &41.25 + 0.6563B + 2.75C + 1.82G \\ &- 0.1175BC - 1.40BG - 1.33CG \\ &- 0.6973B - 1.07C^2 - 3.56G^2 \end{aligned} \quad (4)$$

The results of Box-Behnken test ANOVA are shown in Table 13, where *C*, *G*, *BG*, *CG*, and G^2 have highly significant effects on powder rest angle, *B*, C^2 have significant effects on powder rest angle, while the rest parameters have insignificant effects on powder rest angle. The quadratic regression model has a model P<0.001, a coefficient of determination R^2=0.9829, and a calibrated coefficient of determination adjusted R^2=0.9609, both close to 1 and a coefficient of variation C.V.=1.68%. In summary, the regression model is exceptionally significant and can be further analysed for the rest angle prediction.

Simulation parameter calibration and test verification

Design-Expert 11.0 software was used to find the best combination of parameters for the powder simulation by using the physical test rest angle as the target value for the second-order regression equation: powder-powder static friction coefficient of 0.887, the powder-powder rolling friction coefficient of 0.319, and JKR surface energy of 0.162.

To verify the accuracy and reliability of the powder simulation calibration, the rest angle simulation test was conducted with the combination of the above parameters as EDEM simulation parameters. The mean rest angle obtained is 41.27°, with a relative error of 0.991% from the physical test value of 41.69°. The T-test was performed and P=0.942>0.05, indicating no significant difference between the simulation rest angle and the physical test rest angle. The experimental comparison is shown in Figure 10.

a. Simulation test b. Physical tests

Fig. 10 - Test comparison of the angle of repose of powder

CONCLUSIONS

1) Physical tests measured the basic physical parameters of seeds and powder; the contact parameters between seeds and powder were obtained by applying an inclinometer and high-speed camera, the resting angle of powder was measured as 41.69±0.79 by using a resting angle instrument.

2) Based on particle amplification theory, the powder particles were amplified 6 times for simulation tests. The contact parameters between seeds and powder were calibrated by collision bounce test, ramp slip test, and ramp roll test.

3) The rest angle simulation test was conducted using the range of contact parameters obtained from the physical test as the basis for selecting the simulation test parameters. The Plackett-Burman test, the steepest climb test, and the Box-Behnken test were conducted in turn to establish and optimize the second-order regression equation of the significant parameters and the rest angle, and the best combination of simulation parameters was obtained: the powder-powder static friction coefficient was 0.887, the powder-powder rolling friction coefficient was 0.319, and the JKR surface energy was 0.162.

4) The calibrated contact parameters were used to conduct the simulation test again; the T-test of the result data was obtained as P=0.942>0.05, indicating that there was no significant difference between the simulation test results and the physical test results, further verifying the reliability of the simulation parameter combination.

ACKNOWLEDGEMENTS

We acknowledge that this work was supported by the National Natural Science Foundation of China under the project "Research on structural parameters of split-flow hedge sand collector and its internal flow field characteristics (41661058)" and the Natural Science Foundation of Inner Mongolia Autonomous Region under the project "Research on the working parameters of grass seed pill granulation coating and its coating mechanism under the action of the vibration force field (2018MS05023)".

REFERENCES

[1] Afzal I., (2020), Modern Seed Technology: Seed Coating Delivery Systems for Enhancing Seed and Crop Performance. *Agriculture*, Vol. 10, issue 11;

[2] Asaf Z., (2007), Determination of discrete element model parameters required for soil tillage. *Soil and Tillage Research*, Vol 92, issue 1-2, pp. 227-242;

[3] Boac J M., (2010), Material and Interaction Properties of Selected Grains and Oilseeds for Modelling Discrete Particles[J]. *Transactions of the Asabe*, Vol. 53, issue 4, pp.1201-1216;

[4] Feng Y.T., (2009), On upscaling of discrete element models: similarity principles. *Engineering Computations: International Journal for Computer-Aided Engineering and Software*, Vol. 26, issue 6;

[5] Hao Y.L., (2017), Research on Spiral Dense Conveying of Powder Packaging. *Jiangnan University*;

[6] Hu G.M., (2010), *Discrete Element Method Analysis and Simulation of Particle System——Introduction to Industrial Application of Discrete Element Method and EDEM Software*. Wuhan University of Technology Press;

[7] Johnsonkl, (1971), Surface energy and the contact of elastic solids. *Proceedings of the Royal Society of London Series A, Mathematical and Physical Sciences*, Vol. 324, issue 1558, pp. 301-313;

[8] Jaeger H.M., (1996), The physics of granular materials. *Physics Today*, Vol 49, issue 2, pp. 32-38;

[9] Liu Y., (2017), *Study on the relationship between the accumulation and flow characteristics of powder system and the force between particles*. East China University of Science and Technology;

[10] Li Y.X., (2019), Discrete element parameter calibration of wheat flour-based on grain scaling. *Transactions of the Chinese Society of Agricultural Engineering*, Vol 35, issue 16, pp. 320-327;

[11] Luo S., (2018), Vermicompost matrix discrete element method parameter calibration based on the JKR bonding model. *Transactions of the Chinese Society of Agricultural Machinery*, Vol. 49, issue 04, pp.343-350;

[12] LaTosha M. Gibson., (2013), Image analysis measurements of particle coefficient of restitution for coal gasification applications [J] . *Powder Technology*, Vol. 247, pp. 30-43;

[13] M. Van Zeebroeck, E., (2006), The discrete element method (DEM) to simulate fruit impact damage during transport and handling: Model building and validation of DEM to predict bruise damage of apples [J]. *Postharvest Biology and Technology*, Vol. 41, issue 1;

[14] Ma Y.H., (2020), Parameter calibration of discrete element model for alfalfa straw compression simulation. *Transactions of the Chinese Society of Agricultural Engineering*, Vol. 36, issue 11, pp. 22-30;

[15] Mohammadreza A., (2018), A methodology for calibration of DEM input parameters in the simulation of segregation of powder mixtures, a special focus on adhesion. *Powder Technology*;

[16] Mukherjee R., (2018), DEM based computational model to predict moisture induced cohesion in pharmaceutical powders[J]. *International Journal of Pharmaceutics*, Vol 536, issue 1, pp. 301;

[17] Peng C.W., (2020) Parameter calibration of the discrete element simulation model for pig manure organic fertilizer treated by Heishui Fly. *Transactions of the Chinese Society of Agricultural Engineering*, Vol. 36, issue 17, pp. 212-218;
[18] Pachón-Morales, (2019), DEM modelling for flow of cohesive lignocellulosic biomass powders: Model calibration using bulk tests [J]. *Advanced Powder Technology. https://hal.archives-ouvertes.fr/hal-02294258/document*;
[19] Stavrou Alexandros Georgios, (2020), Investigation of Powder Flowability at Low Stresses by DEM Modelling[J]. *Chemical Engineering Science*, Vol. 211;
[20] Sakai M., Abe M., Shigeto Y., et al. (2014), Verification and validation of a coarse grain model of the DEM in a bubbling fluidized bed[J]. *Chemical Engineering Journal*, Vol. 244, pp.33-43;
[21] Thakur S.C, Ooi JY, Ahmadian H. (2016), Scaling of discrete element model parameters for cohesionless and cohesive solid[J].*Powder Technology*, Vol. 293, pp.130-137;
[22] Tamas K., (2018), The role of bond and damping in the discrete element model of soil-sweep interaction[J]. Biosystems Engineering, Vol. 169, pp. 57-70;
[23] Weinhart, Thomas, Labra, et al. (2016), Influence of coarse-graining parameters on the analysis of DEM simulations of silo flow.[J]. *Powder Technology*;
[24] Wu J.S., (2019), Peucedanum praeruptorum seed physical parameters determination and discrete element simulation model parameter calibration. *Journal of Gansu Agricultural University*, Vol. 54, issue 4, pp. 180-189;
[25] Xing J.J., (2020), Parameter calibration of the discrete element simulation model for the granular red soil in Hainan hot area. *Transactions of the Chinese Society of Agricultural Engineering*, Vol. 36, issue 05, pp. 158- 166;
[26] Zhao L.L., (2009), Seed coating and its application in China. *Chinese Agricultural Science Bulletin*, Vol. 25, issue 23, pp. 126-131;
[27] Zeng Z.W., (2021), Application status and the prospect of discrete element method in agricultural engineering research. *Transactions of the Chinese Society of Agricultural Machinery*, Vol 52, issue 04, pp. 1-20;
[28] Zhou L.H., (2017), EDEM simulation and experimental study of vertical screw conveying. *Zhejiang University of Technology*;